RSC Advances

PAPER

View Article Online
View Journal | View Issue

Cite this: *RSC Adv.*, 2014, **4**, 38606

Efficient laser emission from organic semiconductor activated holographic polymer dispersed liquid crystal transmission gratings

Wenbin Huang,[ab] Linsen Chen*[ab] and Li Xuan[c]

Received 22nd May 2014
Accepted 14th August 2014

DOI: 10.1039/c4ra04837g

www.rsc.org/advances

Performances of organic distributed feedback (DFB) lasers made from holographic polymer dispersed liquid crystal (HPDLC) transmission gratings were greatly improved by replacing common laser dye with organic semiconductor poly(2-methoxy-5-(2′-ethyl-hexyloxy)-*p*-phenylenevinylene) (MEH-PPV) as the gain medium. The MEH-PPV layer was laminated between the glass substrate and the HPDLC grating layer. Light interaction for feedback is provided by an evanescent wave spread into the grating layer. The device showed single-mode, TE polarized laser emission with a threshold of only 0.17 μJ per pulse (17 μJ cm^{-2}). Slope efficiencies as high as 4.7% and 6.5% were measured for optical pumping of the device with P polarization and S polarization, respectively. Lasing was also coupled by the grating out of the waveguide and into free space. Furthermore, the output laser wavelength was systematically tuned over a range of 43 nm by varying the grating period. The laser thresholds at different wavelengths trace well with the amplified spontaneous emission spectrum of the MEH-PPV film. In terms of the HPDLC technique, our results show there is still plenty of potential to be exploited for fabricating organic DFB lasers.

Introduction

Organic fluorescent compounds have been revolutionizing laser technology, opening the way to applications hardly accessible by using inorganic lasers.[1–3] Lasers based on organic gain media are shown to have advantages of low cost, flexibility, ease for integration and wavelength tunability across the whole visible range.[4] Application interest for these organic lasers originates from their huge potential for using as optical sources in high-sensitivity spectroscopy,[5] sensors for explosive vapors[6] and ultrafast switches in all-optical data communication.[7] As organic materials enable more flexibility (*e.g.*, easy chemical engineering of molecular structures for desired properties and no requirement for lattice matching conditions) to work as the laser medium, optically pumped organic lasers have already been demonstrated in a variety of resonator structures, such as mircocavities, microrings, microspheres and Fabry–Perot waveguides.[4] There remains another type of resonator called distributed feedback (DFB) structure that receives the most attention in the field of organic lasers. Instead of using mirrors or total reflections for feedback, these resonators reply on coherent interference of backward Bragg scattering at each corrugation of the wavelength-scale periodic microstructures.[8] The long interaction distance between light and the gain medium guarantees low-threshold and high slope efficiency laser operation. Besides, the central lasing wavelength is specifically dependent on the grating period *via* the Bragg equation, thus the DFB resonator has an excellent mode selection capability. DFB resonators have been fabricated by scanning beam lithography, hot embossing technique, UV nanoimprint lithography and interference ablation technique.[4] New fabrication techniques are still in demand for low-cost and large-volume production of organic DFB lasers.

Holographic polymer dispersed liquid crystal (HPDLC) gratings are fabricated by exposure of the prepolymer mixture which mainly contains light-sensitive monomers and liquid crystal (LC) under the interference pattern created by two or multiple coherent laser beams. The preferential polymerization of the monomers in bright regions would "squeeze" the unreacted LC molecules into dark regions. At some point, accumulated LCs in dark areas is no longer miscible with monomers, leading to a phase separation from the polymer matrix. In this way, the periodically varying intensity of the holographic pattern can be conveniently recorded into the light-sensitive mixture and a wavelength-scale microstructure with alternating layers of LC and polymer is formed. The HPDLC technique for nanofabrication has several advantages, such as easy experimental setup, rapid formation (60 s) and large area (2 cm × 2 cm).[9] Since LC molecules could be reoriented under

[a]*College of Physics, Optoelectronics and Energy & Collaborative Innovation Center of Suzhou Nano Science and Technology, Soochow University, Suzhou, 215006, China. E-mail: lschen@suda.edu.cn*

[b]*Key Lab of Advanced Optical Manufacturing Technologies of Jiangsu Province & Key Lab of Modern Optical Technologies of Education Ministry of China, Soochow University, Suzhou, 215006, China*

[c]*State Key Laboratory of Applied Optics, Changchun Institute of Optics, Fine Mechanics and Physics, Chinese Academy of Sciences, Changchun, 130033, China*

external stimulus, the diffractive properties of these microstructures can be electrically or thermally modulated.

HPDLC gratings were found to be able to work as DFB resonators and show the promise for low-cost and large-volume production of organic lasers.[10] Laser dye was chosen as the gain medium and dissolved into the prepolymer mixture. After the holographic recording process, dye molecules were naturally doped into the grating. Under optical pumping, DFB lasing have be demonstrated in HPDLC reflection gratings,[11] transmission gratings[12–15] and even two-dimensional gratings.[16,17] Thermal and electrical switching properties of lasing from these dye-doped HPDLC DFB lasers have been extensively studied.[10,18–20] Apart from these studies, many attempts have been made to enhance the lasing performance: The laser threshold was first reduced to 5 μJ per pulse by decreasing the size of LC domains[21] and further reduced to 1.35 μJ per pulse by exploiting the Forster energy transfer mechanism;[22] correspondingly, the slope efficiency was reported to increase from 0.1% (ref. 12) to 0.7%.[22] However, the working performance of these HPDLC lasers is still very poor and we attribute it to the used gain medium. It is well known that laser dye molecules suffer severely from concentration quenching,[2] and they can only be doped into the HPDLC grating at a very low concentration (1%) to main high photoluminescence quantum yield (PLQY). As a result, the absorption efficiency of the device is very low and not sufficient gain can be experienced by the resonating lasing mode.

Unlike the laser dye, organic semiconductors could retain very high PLQY even as neat films. They also show large cross-sections for stimulated emission and behave as quasi-four-level laser materials in which the population inversion condition can be easily achieved.[4] In our recent publication,[23] we have designed a new DFB working structure called external feedback scheme to introduce conjugated polymer into HPDLC DFB lasers as the gain medium. Output lasing with a linewidth of 0.7 nm was achieved from this new laser device. In this work, we demonstrate that superior lasing performance can be achieved after optimizing the device parameters: The lasing threshold can be as low as 0.17 μJ per pulse (17 μJ cm^{-2}) at 621.4 nm (one eighth of the lowest in dye-doped HPDLC lasers) and the slope efficiency reaches 6.5% under S polarization pumping (over eight times higher than that in most efficient dye-doped HPDLC lasers). We also show that the single lasing peak could be tuned from 610 nm to 653 nm by changing the grating period. The spectral properties are explained under the DFB waveguide theory and laser thresholds at different wavelengths have also been investigated.

Experimental details

Device preparation

Conjugated polymer poly(2-methoxy-5-(2′-ethyl-hexyloxy)-*p*-phenylenevinylene) (MEH-PPV), one type of organic semiconductor, was chosen as the gain medium. MEH-PPV films have already been demonstrated good lasing properties and they can be simply deposited from solution by spin-coating or ink-jet printing.[24] As the high molecular-weight conjugated polymer is immiscible with the HPDLC mixture, we have employed the external feedback structure here. The fabrication process of the MEH-PPV activated HPDLC laser is shown in Fig. 1. MEH-PPV with an average Mw of ~120 000 (from Jilin OLED Material Co., Ltd) was used as received. Toluene solution containing MEH-PPV (6 mg ml^{-1}) was prepared and spin-coated over a glass substrate (1800 rpm; 30 s). The substrate was then purged under pure nitrogen for several minutes to eliminate the residual solvent. This process leaves a MEH-PPV layer on top of the glass substrate with a thickness of ~80 nm as measured by a DekTak profilometer (I). An empty cell was then made using a pair of glass substrates where the cell gap was controlled as ~6 mm by plastic spacers. Only one of the substrates was with the coated MEH-PPV layer and the other uncoated glass servers as the window for holographic recording (II). The typical HPDLC prepolymer syrup, which consists of 29 wt% monomer dipentaerythritol hydroxyl pentaacrylate (DPHPA), 29 wt% monomer phthalic diglycol diacrylate (PDDA), 10 wt% cross-linking monomer *N*-vinylpyrrolidone (NVP), 0.5 wt% photo-initiator Rose Bengal (RB), 1.5 wt% coinitiator *N*-phenyglycine (NPG) and 30 wt% nematic LC TEB30A (ordinary refractive index = 1.522; extraordinary refractive index = 1.692), was stirred in dark for 24 h to obtain a homogeneously blended mixture. One droplet of the HPDLC mixture was then injected into the cell by capillary effect in the dark. After that, the cell was laid statically in a dark box for several minutes to avoid mixture convection (III). The sample was then placed under the interference field created by two coherent laser beams from a 532 nm Nd-YAG laser source for 2 min (IV). The transmission HPDLC grating spacing Λ can be calculated using $\Lambda = \lambda_w/2 \sin(\theta/2)$, where θ is the intersection angle between the two beams. A low exposure intensity of 8 mW cm^{-2} per beam was used in order to obtain the scaffolding morphologic grating in which LC molecules phase separate to form pure slices.[25] This grating shows a scattering loss less than 4% and is quite suitable for using as the laser cavity. Finally, the DFB device with the external feedback

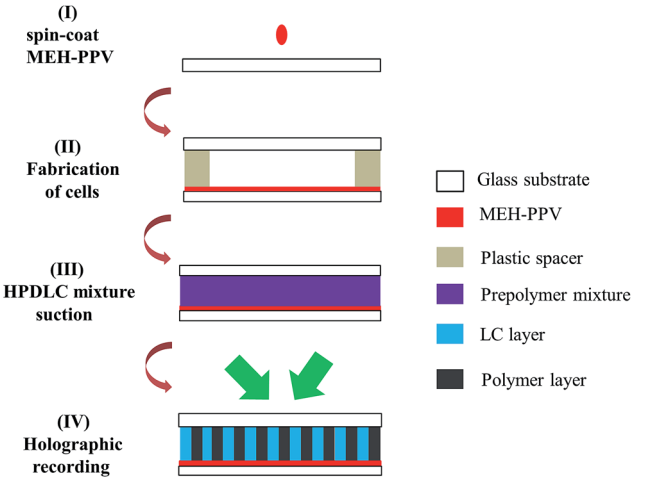

Fig. 1 The fabrication process of the organic semiconductor activated HPDLC DFB laser. (I) Spin-coating the MEH-PPV film onto the substrate. (II) Fabrication of glass cells. (III) Injection of the prepolymer syrup into the cell. (IV) Exposure of the sample under the interference pattern.

structure is completed in which the HPDLC grating lies separately on top of the MEH-PPV layer. It can be seen that the fabrication procedure for MEH-PPV activated HPDLC lasers adds no complexity and the only difference from the dye-doped HPDLC laser is that one glass substrate was deposited with a thin film of conjugated polymer before the cell fabrication. Thus these organic lasers still enjoy advantages of easy experimental setup, large area and low cost.

For a direct observation of the working structure, laser scanning confocal microscopy (LSCM) study was carried out. The glass cell was reopened and the cured films were flushed using ethanol for 10 min to remove the LCs. The films were then cut along the direction perpendicular to grating channels and mounted on the test board with the cross-section upward. The cross-section of the films was then analyzed by the OLYMPUS OSL4000 LSCM. In order to discriminate between the HPDLC grating layer and the MEH-PPV layer, a white light source was used. Compared with scanning electron microscopy study, LSCM requires no coating of an additional conductive layer and the detecting photons would not influence the morphology of the fragile organic films.

Optical characterization

For absorption, photoluminescence (PL) and amplified spontaneous emission (ASE) measurements of the MEH-PPV film, a sample without the grating structure was fabricated. Instead of holographic recording, the prepolymer mixture was exposed using a single laser beam with an intensity of 20 mW cm^{-2} resulting in a film with LC domains randomly distributed in the polymer matrix (polymer dispersed liquid crystal). Absorption and PL measurements were carried out in a Shimadzu UV-3101 spectrophotometer and a Hitachi F-4500 fluorimeter, respectively. ASE properties were explored by optical excitation with a frequency-doubled pulsed Nd-YAG laser at 532 nm (1 Hz, 8 ns). The beam was shaped by a cylindrical lens into a strip of 10 mm by 0.1 mm before impinging upon the sample. ASE emission from the film edge was collected by a fiber coupled spectrometer with a resolution of 0.25 nm.

Fig. 2 shows the optical setup for investigating the emission properties of MEH-PPV activated HPDLC lasers. The frequency doubled pulsed Nd-YAG laser was used as the pump source. The pump energy upon the device was monitored instantaneously by an energy meter collecting one of the split pump beams and can be controlled using a set of neutral filters. A half-wave plate was placed in the optical path to alter the polarization of the pump beam. S polarization is along the *y* axis and P polarization is along the *x* axis. The other pump beam shaped by the cylindrical lens was incident upon the sample to the normal of the cell. Lasing was coupled out from the cell surface and was deflected away from the incident pump beam. Output emission was collected by a spectrometer with a resolution of 0.25 nm. Output lasing energy was measured using a highly sensitive Coherent J-10SI-HE energy meter. The detector with a diameter of 10 mm was placed at around 1 cm from the sample to let all output energy in.

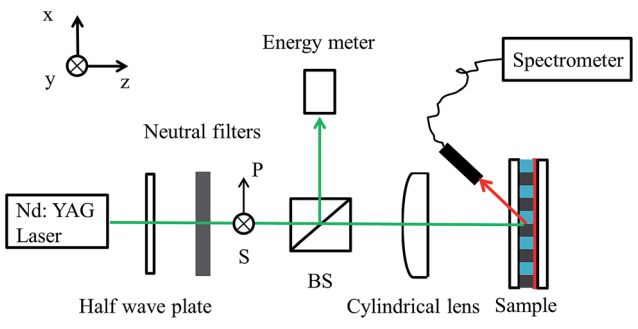

Fig. 2 The optical setup for pumping the MEH-PPV activated HPDLC lasers and collecting the outcoupled emission.

Results and discussions

Optical properties of the pure MEH-PPV layer

The spectroscopic properties of the MEH-PPV solid film are illustrated in Fig. 3 and each spectrum has been normalized to its peak intensity. The absorption of the film peaks at around 495 nm and strong absorption at the pump wavelength of 532 nm can also be anticipated. A quantitative measurement showed that 80% of pulsed pump energy can be absorbed by the 80 nm thick gain medium layer. The high absorption efficiency of conjugated polymer is superior to that of the dye-doped HPDLC film (about 30% during an optical path of 6 μm) and could ensure much higher optical gain. The PL spectrum peaks at 590 nm and there is a shoulder near 620 nm. The spectral overlap (from 500 nm to 600 nm) between absorption and PL bands means that self-absorption loss is significant and lasing action cannot be achieved below 600 nm. ASE is the emission from the film edge without the presence of the grating structure under pulsed optical pumping. It peaks at 620 nm and shows a substantial line-narrowing (a half width of 8 nm) compared with the PL spectrum. ASE results from the amplification of spontaneously emitted photons *via* the stimulated emission process when they are waveguided along the pump strip.[26] Thus ASE contains a significant portion of stimulated emission and can be seen as an indicator of the lasing performance of the gain medium.[27] We anticipate that lasing at around 620 nm gives highest performance and the grating period has to be carefully selected.

Output lasing direction

The grating period was selected to be 580 nm which requires an intersection angle of 54.6°. Fig. 4(a) shows the LSCM image of

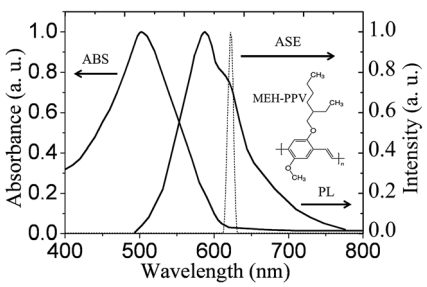

Fig. 3 Absorption, PL and ASE spectra of the MEH-PPV film.

the cross-section of the films. The white LED source instead of a laser source was used in order to tell the red MEH-PPV film from the "transparent" HPDLC grating layer. This is done at the cost of the image spatial resolution (roughly from 0.12 μm to 0.3 μm). As a result, the HPDLC grating structure is not clear, but still we can know two things from the image: one is that the MEH-PPV layer adheres tightly to the grating layer which means a conformal contact between the two layers is achieved; the other is that there is grating structure just on top of the MEH-PPV layer as the corrugation penetrates through the 6 μm thick cell. These two points ensure that this external feedback structure could function well, as the two layers are interacted by the evanescent wave which has a quite short penetration length (~0.5 μm). It is also worth to mention here that the thickness of the MEH-PPV layer shown in the image is not correct. The films were not strictly perpendicular to the testing board and the resulting color crosstalk thickens the gain medium layer. The three layered waveguide structure of the device can be easily seen from the cross-section of the films and the refractive index (RI) of each layer is given schematically in Fig. 4(a). The RI of the glass substrate n_0 is measured to be 1.516 by an Abbe refractometer. When serving as a waveguide layer, the RI modulation of the HPDLC grating is not important and the grating layer can be represented by an averaged RI n_{ave} of 1.541.[20] As for the conjugated polymer layer, the rod-like chromophore chains are distributed randomly in the film plane but not to the normal of the film as a result of the spin-coating process. This chain orientation configuration brings anisotropic optical properties for the film:[28] at 620 nm, TE light would experience a n_1 of 1.92, while the RI for TM light is 1.55. As is clear from the RI of each layer, the MEH-PPV layer works

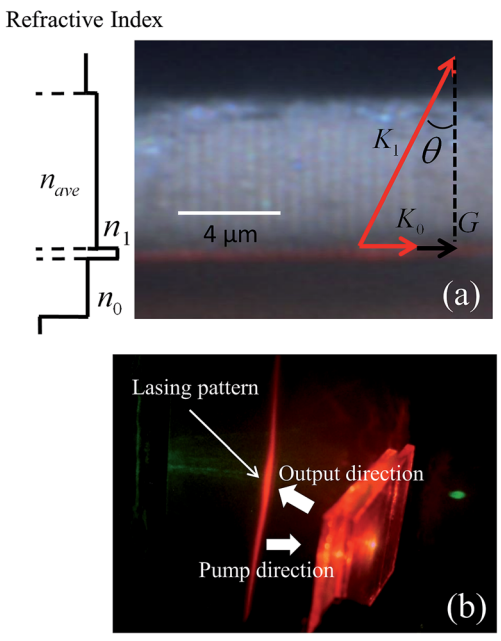

Fig. 4 (a) LSCM image of the cross-section of the films. The sketched triangle shows the output coupling mechanism of the grating. (b) Photo of the operating device pumped by the pulsed laser.

the waveguide core layer while the HPDLC grating layer and the glass substrate function as the cladding layers. The thickness of the conjugated polymer layer has to be experimentally optimized to obtain the best lasing performance.[23] It has to be thin enough to ensure that there is sufficient evanescent wave spread into the HPDLC grating layer, thus optical feedback for a specific lasing mode can be obtained by the coherent interference of backward scattering light at each grating period. In the meanwhile, the waveguide core layer has to be thick enough in order to allow a decent confinement of the lasing mode and photons can be effectively amplified in the gain medium through the stimulated emission process. The HPDLC grating layer on top of the conjugated polymer layer also serves as natural encapsulation to protect it from oxygen and moisture in the air. Thus a long working lifetime in the range between 10^6 and 10^7 pulses (ref. 29) can be anticipated.

Fig. 4(b) shows the image of the operating sample pumped above the laser threshold. Unlike the situation in dye-doped HPDLC transmission gratings where lasing comes from the film edge,[21] this device emits lasing from the cell surface as a result of the grating outcoupling effect. The lasing pattern on the paper screen shows an arc line profile with most of energy concentrated in the center. It is quite divergent along the grating channels while is almost diffraction-limited along the grating vector. Symmetrically, there are four beams of lasing from the device, but only one beam is shown in Fig. 4(b). The outcoupling process is independent of the feedback process and is sketched in Fig. 4(a). The grating would exert a Bragg vector $\vec{G}$ on the original wave vector $\vec{K_0}$, which couples the lasing into the free space with a new wave vector $\vec{K_1}$. According to the momentum conservation in the plane of the waveguide, there would be:[30]

$$\frac{2\pi}{\lambda}\sin(\theta) = \pm\frac{2\pi n_{\text{eff}}}{\lambda} \pm m'\frac{2\pi}{\Lambda} \quad (1)$$

Where λ is the lasing wavelength, n_{eff} is the effective RI of the lasing and m' is the order of the grating coupling. Considering the lasing wavelength fulfills the Bragg equation and we have employed the third order feedback, there is $\lambda = 2n_{\text{eff}}\Lambda/3$. Put this into eqn (1), we have:

$$\sin(\theta) = \left(\pm 1 \pm \frac{2}{3}m'\right)n_{\text{eff}} \quad (2)$$

Restricted by $|\sin(\theta)| \leq 1$, m' can only take the value of 1 or 2, thus:

$$\sin(\theta) = \frac{1}{3}n_{\text{eff}} \approx 0.53 \quad (3)$$

Lasing is coupled out of the waveguide at an angle of 32° with respect to the cell normal, which is in accordance with the experimental result. The surface-emitting output is more suitable for energy extraction as the emission profile is not dependent on the low optical quality edges of the fragile amorphous films.[31] If two-dimensional gratings are used, the output lasing pattern property could be further improved with a low divergence angle at both directions.[32]

Lasing performance

Fig. 5 shows the emission spectrum of the MEH-PPV activated DFB laser pumped above the working threshold. The full width at half maximum (FWHM) of the emission peak is 0.5 nm limited by the resolution of the spectrometer. It is much sharper than the ASE peak from a sample without the grating structure as shown in Fig. 3, giving solid evidence to lasing operation. There is only one lasing peak locating at 621.4 nm. Single mode laser operation can be conveniently achieved in this new device as the MEH-PPV layer which functions as the waveguide core layer is very thin and can only support one propagating lasing mode.[33] It is in stark contrast with the situation in dye-doped lasers in which the very thick HPDLC layer works as the waveguide core layer and several lasing peaks can be found in the output emission.[20,34] The output emission of this new device also contains no parasitic light (*e.g.* ASE emission) which means spontaneous emission has been effectively suppressed by the supported lasing mode. The inset of Fig. 5 shows the dependence of emission intensity on pump energy. Above the laser threshold, the regime of spontaneous emission is switched to stimulated emission. The FWHM of the emission quickly narrows down and the slope of the peak intensity as a function of pump energy instantaneously increases. The inset shows the laser threshold of the new device is around 0.17 μJ per pulse (17 μJ cm^{-2}) which is just one eighth of the lowest in dye-doped HPDLC lasers.[22] The performance of the MEH-PPV activated laser goes beyond our expectation, as the absorption efficiency increases just by 3 times. The reason may lie in the difference in optical scattering property between the HPDLC grating and the MEH-PPV layer. Compared with the homogeneous conjugated polymer layer, scattering loss of the scaffolding morphologic HPDLC grating is still much higher. In the external working structure, although the optical feedback is still provided by the HPDLC grating, the photons experiencing amplification are in the homogeneous MEH-PPV layer. Thus the effect of optical scattering of the grating on laser performance can be alleviated and a much higher improvement can be obtained.

In order to measure the polarization state of output lasing, a polarizer was placed between the detector of the spectrometer and the sample. When the polarization direction was along the *y* axis (as shown in Fig. 2), the polarizer was set to be 0°. Transmitted intensity of output lasing as a function of the rotation angle α of the polarizer is shown in Fig. 6 as solid spheres. The curve is a theoretical plot showing $I = E_0 \cos^2 \alpha$, where E_0 is the intensity when the polarizer angle is set to be 0°. It is clear from the experimental data that the output lasing from the organic semiconductor activated HPDLC laser is totally TE polarized. The linear polarization output can be attributed to the anisotropic optical properties of the MEH-PPV layer. It has been mentioned in the last section that TE light would experience a quite larger RI compared with that of TM light in the conjugated polymer film. The TE lasing mode could be more effectively confined in the gain medium and it would be preferentially amplified. In short, the TM mode is suppressed by the TE mode and energy has been channeled into the TE lasing mode. While in dye-doped HPDLC lasers, both TE and TM polarizations are present as a result of isotropic RI for light propagating along the grating vector.[13] From the perspective of device application, the linearly polarized lasing is certainly more preferred.

Fig. 7 shows output lasing energy as a function of incident pump energy. We found the output *versus* input characteristics of the device are dependent on the pump polarization, so the results for different pump polarizations are also shown. It is worth to mention here that the output lasing wavelength and polarization are not affected by the pump polarization. The solid squares are experimental data, while the three curves are linear fit to the corresponding data. The slope of these linear lines give slope efficiencies while their intersection with the pump energy axis gives laser threshold. The output slope efficiency is lowest 4.7% when the pump light is P polarized, and an intermediate value of 5.9% is obtained when the pump is 45° polarized, while it is the highest 6.5% in the case of S polarized pump. Correspondingly, the laser threshold under P polarization pump is the highest 0.22 μJ per pulse, and is 0.17 μJ per pulse in the case of 45° pumping, while a lowest value of 0.15 μJ per pulse can be obtained under S light.

The pump polarization dependency can be qualitatively explained by the anisotropic distribution of excitations under linearly polarized pump light.[35] The absorption cross-section of the rod-like chromophore molecule depends on its orientation relative to pump polarization.[36] To be more specific, the chromophore molecule absorbs incident photons most efficiently when its principal axis is parallel to the polarization direction of pump light. As a result, the chromophore molecules along the *y*

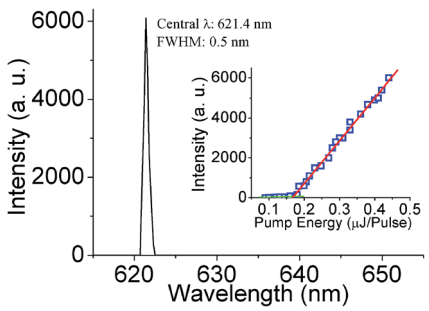

Fig. 5 Emission spectrum of the MEH-PPV activated DFB laser excited at 2.6 × E_{th}. The inset shows the peak intensity as a function of pump energy.

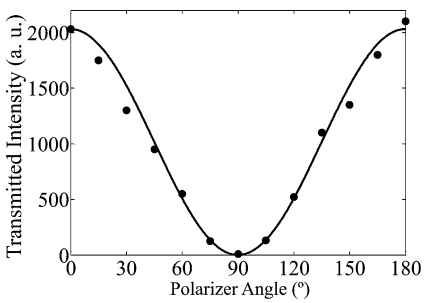

Fig. 6 Transmitted intensity of output lasing through a polarizer as a function of the polarizer angle.

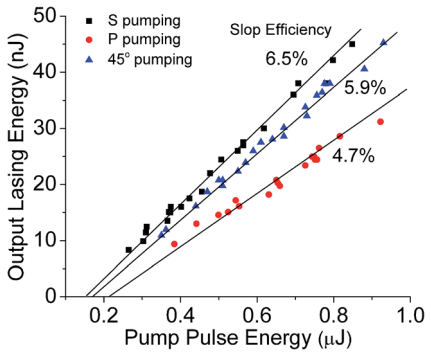

Fig. 7 Output lasing energy as a function of incident pump energy for different pump polarizations.

direction are most effectively excited under S polarization pumping. In the meanwhile, these excited molecules are apt to emit photons with TE polarization (again along the molecule principle axis), which means the stimulation emission cross-section of these anisotropic excitations for the TE mode is the highest. As the TE mode lasing is predominantly supported by the cavity, S pump would provide feedback photons with the highest optical gain. In this case, the slope efficiency is the highest and the laser threshold is the lowest. The slope efficiency of this device represents the current state-of-art for an HPDLC laser, and it is eight times higher than that in most efficient dye-doped HPDLC lasers.[22] We attribute this to be indicative of the effectiveness of our designed working structure and high optical efficiency of the conjugated polymer. It is also noted that slope efficiencies as high as 7.8% have been demonstrated in a conjugated polymer laser with a complicated 2D feedback structure fabricated from the holographic lithography technique.[37] The slope efficiency of our MEM-PPV activated HPDLC laser is comparable to that value while the fabrication of HPDLC gratings is much simpler. These results show that the HPDLC technique has the potential to replace common sophisticated techniques in fabricating organic DFB laser for low-cost and large-volume production. Based on the result of the effect of pump polarization on the slope efficiency, we anticipate that the lasing performance of the MEH-PPV activated HPDLC laser could be further improved by orienting the chromophore molecules along the *y* axis. This measure would improve both the absorption efficiency of the conjugated polymer film and stimulated emission cross-section for TE photons under S polarization pump.[38] This is the topic of our on-going research.

Broadband spectral tuning

As mentioned above, one of the most attracting features of organic gain media is the broadband gain spectrum and it offers the way to fabrication of broadband amplifiers and highly tunable lasers. Lasing wavelength from organic DFB lasers could be readily selected by changing the grating period or the active film thickness (and hence the effective RI of the guided mode). In conjugated polymer lasers, the latter method was often employed[33,39] as common fabrication techniques allow no easy control of the grating pitch. But the variation in the active film has direct influence on mode confinement, absorption efficiency and even number of lasing modes, preventing an easy comparison between lasers at different wavelengths. We demonstrate here the broadband wavelength tuning of the conjugated polymer laser by altering the HPDLC transmission grating period (*via* changing the intersection angle of curing beams) while keeping the active film thickness a constant. As is shown in Fig. 8, output lasing wavelength was tuned from 610 nm to 653 nm when the grating period was varied from 566.5 nm to 615.6 nm. Outside this range, no lasing peak can be observed showing the width of tunable range of the MEH-PPV film is around 43 nm. No additional higher lasing modes can be found in these emission spectra, as the active film thickness was kept as thin as 80 nm to allow only the lowest propagating mode being confined. At the edge of the gain band, either at 610 nm or 653 nm, the emission spectrum contains not only the single lasing peak but also some ASE background. The parasitic light arises due to low optical gain at edge wavelengths where the spontaneous emission cannot be well suppressed by the lasing mode: At the short wavelength edge, the self-absorption by the gain medium cannot be neglected which brings additional loss; while at the long wavelength edge, the low optical gain is due to decreased stimulated emission cross-section of excitations. The associated laser thresholds at different wavelengths have also been determined and are shown in Fig. 9. It can be seen that the lowest threshold is 0.17 μJ per pulse which operates at 621 nm. This location is consistent with the ASE peak where the net gain is the highest. The threshold increases rapidly as the lasing wavelength approaches the short edge of the ASE spectrum. At the shortest lasing wavelength of 610 nm, the laser threshold increases by six times and reaches 1.3 μJ per pulse. This shows that self-absorption loss plays an important role in determining the tunable range of output lasing. We anticipate that performance of this new laser could be further improved by adopting the Forster energy transfer scheme as it would move the absorption spectrum of the gain medium away from its emission spectrum.[40]

The dependence of lasing wavelength on the HPDLC grating period can be further explained under the mode selection mechanism of the DFB laser.[20] The supported lasing mode has to fulfill two requirements. One is that it should be the

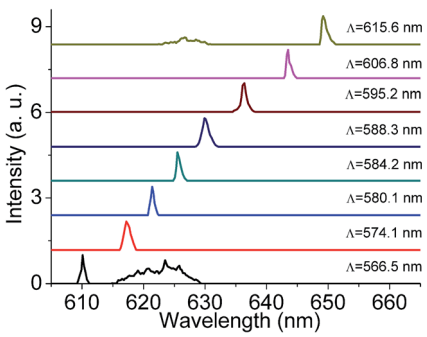

Fig. 8 Laser emission spectra from MEH-PPV activated HPDLC lasers with different grating periods.

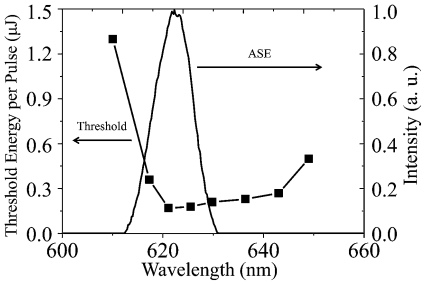

Fig. 9 Oscillation thresholds at a function of output lasing wavelength. The ASE spectrum is also shown for comparison.

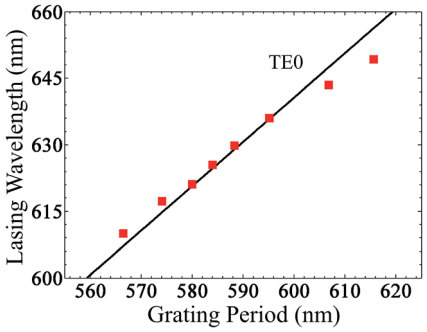

Fig. 10 The dependence of lasing wavelength on the grating period. Squares are experimental data. The solid curve is the calculation based on the DFB waveguide theory.

propagating mode in the MEH-PPV layer which functions as the waveguide core layer. Thus the optical mode can be confined in the gain medium and will not leak out through above and below cladding layers; the other is that the mode wavelength has to fulfill the DFB Bragg equation. In this way, the coherent interference of backward scattered light at each grating period can be obtained which is a prerequisite for laser action. The well-known asymmetrical TE waveguide equation[41] with the parameters shown in Fig. 4(a) is:

$$\frac{2\pi h}{\lambda}\sqrt{{n_1}^2-{n_{\text{eff}}}^2}=m_{\_\text{mode}}\pi+\tan^{-1}\sqrt{\frac{{n_{\text{eff}}}^2-{n_{\text{ave}}}^2}{{n_1}^2-{n_{\text{eff}}}^2}}+\tan^{-1}\sqrt{\frac{{n_{\text{eff}}}^2-{n_{\text{ave}}}^2+\gamma\left({n_1}^2-{n_{\text{ave}}}^2\right)}{{n_1}^2-{n_{\text{eff}}}^2}} \quad (4)$$

Where λ is the mode wavelength, n_1 is the RI of the MEH-PPV layer (1.92 for TE mode at 620 nm), h is the thickness of the core layer (80 nm), n_{eff} is the effective RI of the mode, $m_{\_\text{mode}}$ is the order of the propagating mode (0, 1, 2…) and γ equals $({n_{\text{ave}}}^2-{n_0}^2)/({n_1}^2-{n_{\text{ave}}}^2)$ which is a measure of the asymmetry of the waveguide. Taking into account that the effective RI is linked to Λ by the third-order Bragg equation $2n_{\text{eff}}=3\lambda/\Lambda$, the dependency of lasing wavelength λ on Λ can be numerically solved and is shown as the solid curve in Fig. 10. The solution arises only when $m_{\_\text{mode}}$ takes the value of 0 which means only the lowest TE_0 mode can be supported by the cavity. The experimental data in Fig. 8 are shown as squares in Fig. 10. The experimental data agree with the theoretical curve very well when the lasing wavelength is between 620 nm and 635 nm while deviate from it at both short and long wavelength edges. This is because we haven't taken RI dispersion of the MEH-PPV film into consideration. According to literature,[28] RI of the MEH-PPV film should be higher and lower than 1.92 at 610 nm and 650 nm, respectively. Thus, better agreement can be obtained based on the waveguide DFB laser theory if the RI dispersion of the gain medium is taken into account. Our initial intention was to fabricate electrically tunable conjugated polymer activated HPDLC grating lasers. But no wavelength tuning was demonstrated under applied electric field in experiments. Later we found the supported lasing mode could only experience the ordinary RI in the LC layer when LC molecules are rotating in the plane perpendicular to the glass substrate. Because the supported lasing mode is TE polarized and the initial LC molecules are oriented along the grating vector. Deliberate structure designs are required to overcome this limitation to fully make use of the tunability of the grating.

Conclusions

We have given a full optimization and characterization of the lasing performance of MEH-PPV activated HPDLC lasers. The MEH-PPV layer was laminated between the glass substrate and the HPDLC transmission grating layer to replace common laser dye as the new gain medium. Profited from the high absorption efficiency of the conjugated polymer and the effectiveness of the external feedback structure, the performance of the laser is greatly improved. It emits single-mode, totally TE polarized laser emission. Output lasing was also coupled by the grating out of the waveguide and is more convenient for energy extraction. The operation threshold at 621.4 nm was 0.17 μJ per pulse (17 μJ cm^{-2}) which is just one eighth of the lowest in dye-doped HPDLC lasers. It is further found S pump polarization gives a high slope efficiency of 6.5% which is over eight times higher than that in most efficient dye-doped HPDLC lasers. The lasing wavelength can be conveniently tuned from 610 nm to 653 nm by varying the grating period showing a wide gain band of the MEH-PPV film. This work also implies that lasing performance of HDPCL lasers can be further improved by adopting three measures: using 2D HPDLC gratings as resonators, orientating chromophore chains of the conjugated polymer along the specific direction and employing the Forster energy transfer scheme to decrease self-absorption loss. Our results establish the HPDLC technique as a promising route to the realization of low-cost and large-volume production of efficient organic DFB lasers.

Acknowledgements

The authors gratefully acknowledge financial support from the Priority Academic Program Development of Jiangsu Higher Education Institutions (PAPD).

Notes and references

1 S. Chénais and S. Forget, *Polym. Int.*, 2012, **61**, 390–406.

2 M. D. McGehee and A. J. Heeger, *Adv. Mater.*, 2000, **12**, 1655–1668.
3 G. Kranzelbinder and G. Leising, *Rep. Prog. Phys.*, 2000, **63**, 729–762.
4 I. D. W. Samuel and G. A. Turnbull, *Chem. Rev.*, 2007, **107**, 1272–1295.
5 T. Woggon, S. Klinkhammer and U. Lemmer, *Appl. Phys. B*, 2010, **99**, 47–51.
6 Y. Yang, G. A. Turnbull and I. D. W. Samuel, *Adv. Funct. Mater.*, 2010, **20**, 2093–2097.
7 J. Clark and G. Lanzani, *Nat. Photonics*, 2010, **4**, 438–446.
8 H. Kogelnik and C. V. Shank, *Appl. Phys. Lett.*, 1971, **18**, 152–154.
9 V. P. Tondiglia, L. V. Natarajan, R. L. Sutherland, D. Tomlin and T. J. Bunning, *Adv. Mater.*, 2002, **14**, 187–191.
10 R. Jakubiak, T. J. Bunning, R. A. Vaia, L. V. Natarajan and V. P. Tondiglia, *Adv. Mater.*, 2003, **15**, 241–244.
11 D. E. Lucchetta, L. Criante, O. Francescangeli and F. Simoni, *Appl. Phys. Lett.*, 2004, **84**, 4893–4895.
12 V. K. S. Hsiao, C. Lu, G. S. He, M. Pan, A. N. Cartwright, P. N. Prasad, R. Jakubiak, R. A. Vaia and T. J. Bunning, *Opt. Express*, 2005, **13**, 3787–3794.
13 Y. J. Liu, X. W. Sun, P. Shum, H. P. Li, J. Mi and W. Ji, *Appl. Phys. Lett.*, 2006, **88**, 061107.
14 D. E. Lucchetta, F. Vita, R. Castagna, O. Francescangeli and F. Simoni, *Photonics and Nanostructures – Fundamentals and Applications*, 2012, **10**, 140–145.
15 G. Strangi, V. Barna, R. Caputo, A. De Luca, C. Versace, N. Scaramuzza, C. Umeton, R. Bartolino and G. N. Price, *Phys. Rev. Lett.*, 2005, **94**, 063903.
16 R. Jakubiak, V. P. Tondiglia, L. V. Natarajan, R. L. Sutherland, P. Lloyd, T. J. Bunning and R. A. Vaia, *Adv. Mater.*, 2005, **17**, 2807–2811.
17 D. Luo, X. W. Sun, H. T. Dai, Y. J. Liu, H. Z. Yang and W. Ji, *Appl. Phys. Lett.*, 2009, **95**, 151115.
18 D. Luo, X. W. Sun, H. T. Dai, H. V. Demir, H. Z. Yang and W. Ji, *J. Appl. Phys.*, 2010, **108**, 013106.
19 R. Jakubiak, L. V. Natarajan, V. Tondiglia, G. S. He, P. N. Prasad, T. J. Bunning and R. A. Vaia, *Appl. Phys. Lett.*, 2004, **85**, 6095–6097.
20 W. Huang, Z. Diao, L. Yao, Z. Cao, Y. Liu, J. Ma and L. Xuan, *Appl. Phys. Express*, 2013, **6**, 022702.
21 Y. J. Liu, X. W. Sun, H. I. Elim and W. Ji, *Appl. Phys. Lett.*, 2007, **90**, 011109.
22 L. Liu, W. Huang, Z. Diao, Z. Peng, Q. Mu, Y. Liu, C. Yang, L. Hu and L. Xuan, *Liq. Cryst.*, 2014, **41**, 145–152.
23 W. Huang, Z. Diao, Y. Liu, Z. Peng, C. Yang, J. Ma and L. Xuan, *Org. Electron.*, 2012, **13**, 2307–2311.
24 G. A. Turnbull, P. Andrew, W. L. Barnes and I. D. W. Samuel, *Appl. Phys. Lett.*, 2003, **82**, 313–315.
25 W. Huang, Y. Liu, Z. Diao, C. Yang, L. Yao, J. Ma and L. Xuan, *Appl. Opt.*, 2012, **51**, 4013–4020.
26 M. D. McGehee, R. Gupta, S. Veenstra, E. K. Miller, M. A. Díaz-García and A. J. Heeger, *Phys. Rev. B: Condens. Matter Mater. Phys.*, 1998, **58**, 7035–7039.
27 E. M. Calzado, P. G. Boj and M. A. Díaz-García, *Materials*, 2009, **2**, 1288–1304.
28 M. Tammer and A. P. Monkman, *Adv. Mater.*, 2002, **14**, 210–212.
29 S. Richardson, O. P. M. Gaudin, G. A. Turnbull and I. D. W. Samuel, *Appl. Phys. Lett.*, 2007, **91**, 261104.
30 G. A. Turnbull, P. Andrew, M. J. Jory, W. L. Barnes and I. D. W. Samuel, *Phys. Rev. B: Condens. Matter Mater. Phys.*, 2001, **64**, 125122.
31 C. Karnutsch, C. Gýrtner, V. Haug, U. Lemmer, T. Farrell, B. S. Nehls, U. Scherf, J. Wang, T. Weimann, G. Heliotis, C. Pflumm, J. C. deMello and D. D. C. Bradley, *Appl. Phys. Lett.*, 2006, **89**, 201108.
32 S. Riechel, C. Kallinger, U. Lemmer, J. Feldmann, A. Gombert, V. Wittwer and U. Scherf, *Appl. Phys. Lett.*, 2000, **77**, 2310–2312.
33 S. Riechel, U. Lemmer, J. Feldmann, S. Berleb, A. G. Mückl, W. Brütting, A. Gombert and V. Wittwer, *Opt. Lett.*, 2001, **26**, 593–595.
34 M. S. Li, A. Y.-G. Fuh and S.-T. Wu, *Opt. Lett.*, 2012, **37**, 3249–3251.
35 S. A. v. d. Berg, G. W. t. Hooft and E. R. Eliel, *Chem. Phys. Lett.*, 2001, **347**, 167–172.
36 B. Valeur, *Molecular Fluorescence: Principles and Applications*, Wiley-VCH, New York, 2001.
37 G. Heliotis, R. Xia, G. A. Turnbull, P. Andrew, W. L. Barnes, I. D. W. Samuel and D. D. C. Bradley, *Adv. Funct. Mater.*, 2004, **14**, 91–97.
38 R. Xia, M. Campoy-Quiles, G. Heliotis, P. Stavrinou, K. S. Whitehead and D. D. C. Bradley, *Synth. Met.*, 2005, **155**, 274–278.
39 R. Xia, W.-Y. Lai, P. A. Levermore, W. Huang and D. D. C. Bradley, *Adv. Funct. Mater.*, 2009, **19**, 2844–2850.
40 D. Schneider, T. Rabe, T. Riedl, T. Dobbertin, M. Kröger, E. Becker, H.-H. Johannes, W. Kowalsky, T. Weimann, J. Wang and P. Hinze, *Appl. Phys. Lett.*, 2004, **85**, 1659–1661.
41 K. Okamoto, *Fundamentals of Optical Waveguides*, Academic press, Burlington, 2006, 2nd edn.